JOURNAL OF PROPULSION AND POWER
Vol. 11, No. 6, November–December 1995

Installed F/A-18A Inlet Flow Calculations: A Grid Study

C. Frederic Smith* and Steve D. Podleski†
NYMA, Inc., Brook Park, Ohio 44142

Full Navier–Stokes calculations on the F/A-18A High Alpha Research Vehicle inlet at 30 deg angle of attack, 0 deg yaw, and a freestream Mach number of 0.2, have been obtained in this study using an algebraic turbulence model with two grids (original and revised). In addition, a limited set of results were obtained using a thin-layer Navier–Stokes (TLNS) code with the revised grid. The limitedness of the results was due to the inadequacy of the grid to meet the requirements of the TLNS code. Results obtained with the original grid were used to determine where further grid refinements and additional geometry were needed. The calculations are compared to a limited amount of available experimental data. The predicted forebody/fuselage surface static pressures compared well with data for all solutions. The predicted trajectory of the vortex generated under the leading-edge extension was different for each solution. These discrepancies are attributed to differences in the grid resolution, turbulence modeling, artificial dissipation, and differencing schemes. All solutions predict that this vortex is ingested by the inlet. The predicted 40-probe rake inlet total pressure recoveries are lower than data and the distortions are higher than data. The results obtained with the revised grid were significantly improved from the original grid results.

Nomenclature

C_p = $(P - P_\infty)/\frac{1}{2}\rho_\infty V_\infty^2$, static pressure coefficient
$\dot{m}$ = mass flow rate
$(\dot{m}\sqrt{\theta})/\delta$ = corrected flow rate
P = local static pressure
P_T = local total pressure
$P_{T\text{avg}}$ = average total pressure
$P_{T\text{max}}$ = maximum total pressure
$P_{T\text{min}}$ = minimum total pressure
$P_{T\infty}$ = freestream total pressure
P_∞ = freestream static pressure
$T_{T\text{avg}}$ = average total temperature
V_∞ = freestream velocity
α = angle of attack
β = angle of yaw
δ = $P_{T\text{avg}}/(14.696$ lb/in.$^2)$
θ = $T_{T\text{avg}}/519.0$R at compressor face
ρ_∞ = freestream density

Introduction

THE F/A-18A aircraft has experienced engine stalls at high angles of attack and yaw flight conditions during Navy envelope expansion flights. At these flight conditions, high angular rates were also present. Future fighter aircraft may be designed to operate routinely in this flight regime. Therefore, it is essential that an understanding of the inlet flowfield at these flight conditions be obtained. Due to the complex interactions of the fuselage flowfield and the inlet flowfield, a study of the flow within the inlet must also include the external effects.

Past calculations of flow about the F/A-18A have not included the inlet and ramp.[1,2] These features are usually smoothed over and assumed not to influence the external flowfield significantly. However, the effects from the upstream forebody, leading-edge extension (LEX) and diverter must be included in order to provide the proper inflow conditions to the inlet duct.

One of the goals of the NASA high alpha technology program is to accurately predict the aerodynamics of aircraft operating at extreme attitudes (α = 60 deg, β = 10 deg). As part of this program, NASA Dryden, Ames, and Langley are concentrating on external aerodynamics including thrust vectoring control systems and vortex flow control. NASA Lewis is studying the effects of high angle-of-attack and yaw flight conditions on flow within the F/A-18A High Alpha Research Vehicle (HARV) inlet duct. The HARV is a specially equipped F/A-18A aircraft used to study high alpha aerodynamics. Details of this cooperative program are contained in Ref. 3. The effects of rate of change in the angle of attack and yaw will be considered for the flight tests only. The stabilized flight data will be obtained by holding the aircraft at specified conditions for 6 s.

The results of including the inlet and ramp in the flow simulation are reported in Ref. 4. The results of this effort formed the foundation for the work that is reported in this article. The solutions obtained in this previous study were evaluated and several shortcomings were identified. This resulted in obtaining a much more detailed and complete geometry data base of the F/A-18A aircraft and inlet. In addition, several areas of the computational grid were revised to improve flowfield and surface resolution.

Full Navier–Stokes (FNS) calculations on the installed 19.78% scale F/A-18A inlet at 30 deg angle of attack, 0 deg yaw, and a freestream Mach number of 0.2 have been obtained in this study using the PARC3D code[5] with the Baldwin–Lomax algebraic turbulence model. In order to properly account for the external effects, the forebody, LEX, ramp, and wing were included with inlet geometry as shown in Fig. 1a. In the original study, the diverter, LEX slot, and leading-edge flap were not included due to insufficient geometry definition. These were included in the revised geometry as shown in Fig. 1b and the results obtained with both configurations are presented in this report. Results obtained with the original grid were used to determine where further grid refinements and additional geometry were needed. This was done by examining the solution obtained with the original grid for regions where flow gradients weren't resolved well. Also, areas where

Received May 27, 1994; presented as Paper 94-3123 at the AIAA/ASME/SAE/ASEE 30th Joint Propulsion Conference, Indianapolis, IN, June 27–29, 1994; revision received Dec. 12, 1994; accepted for publication Dec. 13, 1994.

*Supervisor, Propulsion Aerodynamics Section, 2001 Aerospace Parkway. Senior Member AIAA.

†Senior Engineer, Propulsion Aerodynamics Section, 2001 Aerospace Parkway. Member AIAA.

Table 1 PARC3D and CFL3D component modeling differences

Component	PARC3D, Version 5.8	CFL3D, Version 2.1
Canopy grid	90 × 33 × 18	41 × 33 × 17
Under LEX grid	82 × 49 × 50	41 × 49 × 49
Inlet highlight	Embedded c-grid	No c-grid
Diverter	Turbulent flow with LEX slot	Laminar flow with exit static pressure boundary condition
Upper diverter	Turbulent flow	Laminar flow
LE flap	Modeled	Not modeled

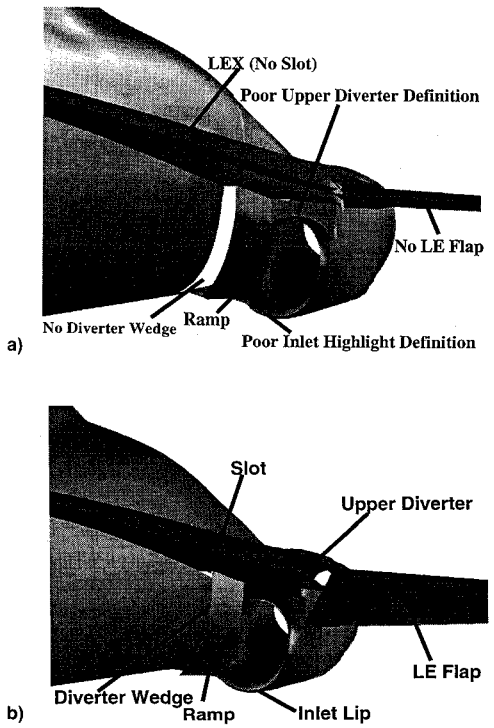

Fig. 1 F/A-18A geometry: a) original and b) revised.

geometry was not modeled were examined to assess whether or not the inclusion of the geometry might influence the flowfield locally. The calculations are compared to data.[6,7] In particular, data for the inlet flowfield is very limited. These results will be more fully compared with data obtained from experimental programs. The purpose of these comparisons is to evaluate/validate the codes. The codes will also be used to aid in the interpretation of the experimental results and provide information concerning the detailed flow structures, which are not normally measured.

In addition, a very limited comparison of the PARC3D results was made with those obtained using another code. The code chosen was CFL3D Version 2.1, (Ref. 8) which has been used extensively for external flow calculations at NASA Langley. This code was used to evaluate the effects on the solution using a code with more recent algorithm developments as described later. The comparison is limited due to the fact that the grid used was generated for PARC3D specifications and does not meet the CFL3D requirements very well. Due to a limited amount of time and resources, it was not possible to generate a grid that fully met the CFL3D requirements or run the CFL3D grid with PARC3D. Therefore, the comparisons made in this article between PARC3D and CFL3D do not provide a sufficient basis to determine the strengths and weaknesses of each code. The actual reason for running CFL3D was to provide some additional corroborating CFD results to support the PARC3D solution, since little data exist for comparison. A comparison of the component modeling differences is shown in Table 1. The use of laminar flow in regions with opposing walls in CFL3D was due to the code requiring the wall index to be 1 for turbulent flow. The exclusion of the leading-edge flap and embedded c-grid was due to CFL3D not being able to accommodate overlayed grids. The reduction in streamwise grid points for CFL3D was to keep the core memory requirements under 30 MWords for the Lewis Cray Y-MP computer.

Numerical Modeling

In this section the major features of the PARC3D and CFL3D codes are presented along with a discussion of the boundary conditions used with each code. A brief discussion of the development of the computational grid is presented.

PARC3D Code

The PARC3D code Version 5.8 (Ref. 5) solves the full three-dimensional Reynolds averaged Navier–Stokes equations in strong conservation form using the Beam and Warming approximate factorization scheme to obtain a block tridiagonal system of equations. Pulliam's scalar pentadiagonal transformation provides for an efficient solver. The code uses the Baldwin–Lomax turbulence model.[9] The PARC version of the turbulence model does not use the streamwise component of vorticity in the determination of the turbulent viscosity.[10] This approach was found to improve the modeling of vortical flows in ducts. The implicit scheme uses central differencing with artificial dissipation to eliminate oscillations in the solution associated with the use of central differences. This code allows for the use of multiple grid blocks. Trilinear interpolation[11] is used to transfer information at the grid block interfaces. Default dissipation values were used (second-order 0.25, fourth-order 0.64).

CFL3D Code

The CFL3D code Version 2.1 (Ref. 8) solves the thin-layer Navier–Stokes (TLNS) equations. It employs the Baldwin–Lomax[9] turbulence model. The equations are solved using upwind differencing with a total variation diminishing (TVD) scheme. The TVD scheme eliminates oscillations due to dispersion errors introduced by the higher-order terms in the upwind differences by shutting off these higher-order terms in regions of large flow oscillations. Various options are available in the code for TVD schemes, flux-vector differencing, and upwinding accuracy. The options chosen were the Roe flux difference splitting scheme, third-order accurate upwinding, and the smooth flux limiter, which is tuned for the third-order accurate upwinding scheme. The three-factor approximate factorization scheme is used to obtain a block tridiagonal system of equations. For the Roe scheme, the equations are diagonalized to obtain a scalar tridiagonal system of equations. This diagonalization provides for a more efficient solver. A semiconservative scheme is employed to transfer information between grid blocks.[12] Multigridding is also available, which may accelerate the convergence of the solution.[13]

Grid Generation

The geometry database used to create the grid for this study was the F/A-18A aircraft. The database consisted of x, y, z coordinate points given at axial cuts along the fuselage. The database included the definition of the fuselage, LEX, wing, tail, ramp, and the inlet. The original grid based on the initial database did not include or have sufficient definition of the diverter, the LEX slot, and the inlet highlight. The deficiencies in the geometry database used for this grid have been corrected, and a revised grid, created with the more accurate database, was generated. The GRIDGEN codes[14] were used to generate the computational grids.

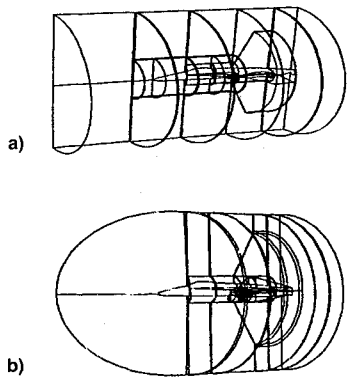

Fig. 2 Grid block structure: a) original and b) revised.

Due to the complex interactions between the fuselage flowfield and the inlet flowfield, the forebody, fuselage, LEX, ramp, and wing were all included in the grid. The horizontal tail, vertical tail, aft fuselage, and the nozzle were not modeled because of their assumed minimal effects on the inlet flowfield.

The wing leading-edge flap, which is deflected down 34 deg when the aircraft is at 30 deg angle of attack and greater, was modeled undeflected in the original grid. The deflected flap was included in the revised grid. An embedded c-grid about the inlet highlight is also included in the revised grid to improve the resolution of flow gradients and surface geometry.

The blocking structure used for the F/A-18A grid consists mainly of o-grids wrapped around the fuselage, in the crossflow plane. The original F/A-18A blocking structure can be seen in Fig. 2a and consisted of 20 blocks. The revised F/A-18A blocking structure is shown in Fig. 2b with 22 blocks. The inlet block is an o-grid extending from the inlet lip to the compressor face. The blocks were created such that the blocks under the LEX contained grids for viscous flows ($y + < 5$), whereas the blocks over the LEX were sparser for inviscid flow analysis. This was done because the viscous effects above the LEX did not significantly effect the flow into the inlet. This also decreased the required number of grid points and, thus, the run times. Blocks were extended approximately one body length away from the surface in order to minimize the effects of the freestream boundary condition on the solution near the inlet. Further details of the grid generation process are contained in Ref. 15.

Boundary Conditions

PARC3D Code

Far-field-type boundary conditions were imposed along the outer computational boundaries. This type of condition uses a one-dimensional Riemann invariant to maintain the freestream flow conditions. Along the windward side of the airframe, no-slip, adiabatic conditions are specified. Along the leeward side of the aircraft, inviscid flow is specified. The static pressure at the engine face was adjusted, using a simulated rake, to obtain the equivalent experimental corrected mass flow rate based upon total pressure at the engine face plane obtained from an average of 40 total pressures in a configuration of 8 equally spaced legs with 5 equal area total pressure locations per leg. Symmetry conditions were assumed along the centerline of the aircraft. Trilinear interpolation is used to transfer data between the grid blocks.

CFL3D Code

The boundary conditions used by CFL3D were similar to the PARC3D conditions with a few exceptions. The CFL3D code does not have a turbulence model with generalized wall boundary conditions that allow the use of opposing walls within a grid block. Therefore, the flow in the diverter, LEX slot, and upper diverter was treated as laminar. Also, since the grid block interface boundary conditions are for a full block surface, the slot exit was modeled as a subsonic exit pressure boundary instead of an interface to the top side of the LEX, since the slot interface made up only a portion of the adjoining block's surface. The exit static pressure was set based upon the average static pressure calculated by the PARC3D code that used an interface boundary condition. In order to model the slot interface similar to the PARC3D code, the use of several grid blocks on the top side of the LEX would be required to isolate the slot interface along a complete grid block surface. Since the flow over the top of the LEX does not significantly affect the flowfield under the LEX, setting the diverter downstream pressure to a value consistent with the slot being present should provide approximately the proper flow rate behind the ramp.

Results

In this section, the results using the original and revised grids with PARC3D and the CFL3D solution are presented. The external flow results are presented first and are followed by a discussion of the inlet duct flowfield predictions. The results are compared with available data. More extensive details of the results are contained in Ref. 15.

External Flowfield

In this section, the external flow features common to all three solutions will be discussed first. Following this, the differences in the three external flow results will be presented. The graphical results presented in this section were obtained using the PLOT3D program.[16]

The predicted particle traces (simulated oil flows) along the forebody and along the fuselage below the LEX are shown in Fig. 3. The windward vortex is generated when the flow impinges on the bottom of the LEX and moves down the fuselage until it reaches a separation line. The PARC3D solution using the revised grid indicates that the under LEX vortex has moved downward along the fuselage as compared to the flow pattern shown for the original grid. The increased curvature in the particle traces using the revised grid may be due to the flow through the slot that causes an upward movement of the traces near the entrance to the diverter region. In addition, the diverter wedge is providing blockage to the flow.

The particle traces obtained using the CFL3D solution with the revised grid are somewhat different than the particle traces

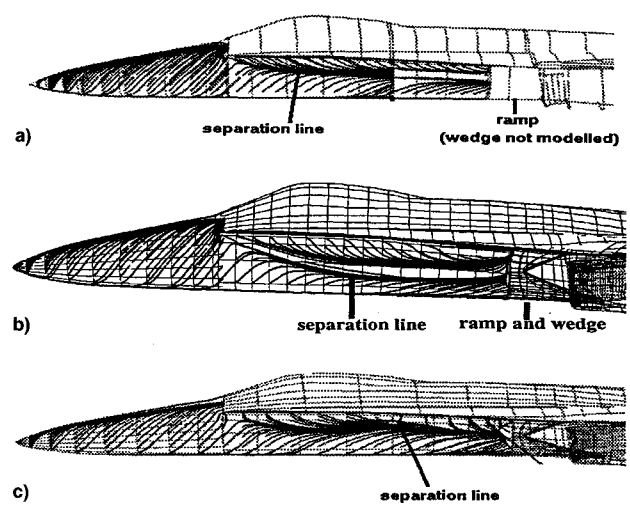

Fig. 3 Particle trajectories along surface: a) PARC3D solution: original grid, b) PARC3D solution: revised grid, and c) CFL3D solution: CFL3D grid.

predicted by PARC3D using the revised grid. These discrepancies between the PARC3D and CFL3D results may be due to the fact that the revised grid used for the CFL3D calculations along the lower LEX region of the fuselage had approximately half the number of streamwise points as the revised PARC3D grid due to the core memory storage limitations of CFL3D. In addition, the version of the Baldwin–Lomax turbulence model used in the PARC3D solutions included only the component of vorticity that is normal to the streamwise direction in the determination of the turbulent viscosity, whereas the CFL3D code uses the total vorticity. This difference can affect the position of the vortex as discussed in Ref. 10. Another source of the discrepancies is the different algorithms used. The PARC3D code uses central differencing with artificial dissipation while the CFL3D code uses a third-order upwinded differencing with a TVD scheme. The amounts of numerical dissipation introduced into the solution by these two schemes could be quite different.

Another effect on the vortex trajectory is due to the modeling of the flow behind the ramp. A comparison to the PARC3D results with the original and revised grids shows that the inclusion of the diverter and slot in the revised grid causes the flow to move slightly upstream from the ramp and upwards through the slot. The flow behind the ramp in the original grid was modeled inviscidly, without a slot or diverter, which resulted in the flow moving parallel to the axial direction. The CFL3D results show a larger region of flow separation ahead of the ramp than the PARC3D results using the revised grid. This discrepancy in the two solutions may be attributed to the use of the laminar flow approximation in the CFL3D solution in the diverter/slot grid blocks. The laminar flow tends to have larger regions of crossflow separation than the turbulent case, and may affect the flow directionality.

Surface static pressure measurements from flight tests[6] were made at several fuselage stations shown in Fig. 4 (F.S. = full-scale inches from reference station).These tests were done to study external aerodynamic problems. As shown in Fig. 5, the numerical results for the surface static pressures along the forebody and under the LEX are all in good agreement with the data,[6] despite differences in the vortex location. The CFL3D results appear to have the closest agreement with the data, although the other solutions are almost as close. The discrepancies between the numerical results and the data along the forebody may be due to the lack of adequate grid resolution of the vortex-dominated region of the flow. Another source for the discrepancies is laminar-to-turbulent transitioning flow that is present on the full-scale vehicle.[6] These calculations assume fully turbulent flow present everywhere and are at model scale. Along the top side of the LEX the agreement is poor due to lack of grid resolution and the use of the inviscid flow approximation.

Inlet Duct Flowfield

In this section, several aspects of the inlet duct flowfield are examined. Comparisons of the predicted surface static pressure distributions about the inlet highlight are first presented. This is followed by a discussion of the predicted total pressure contours at the inlet entrance and engine face. The predicted engine face total pressure contours are compared with experimental total pressure contours. The predicted inlet performance is also compared with data. Further details concerning the inlet duct flowfield are contained in Ref. 15.

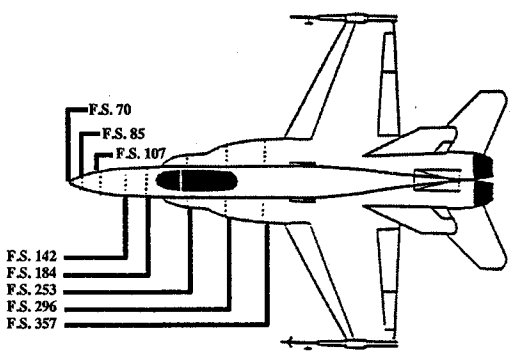

Fig. 4 Forebody/LEX surface pressure measurement stations.

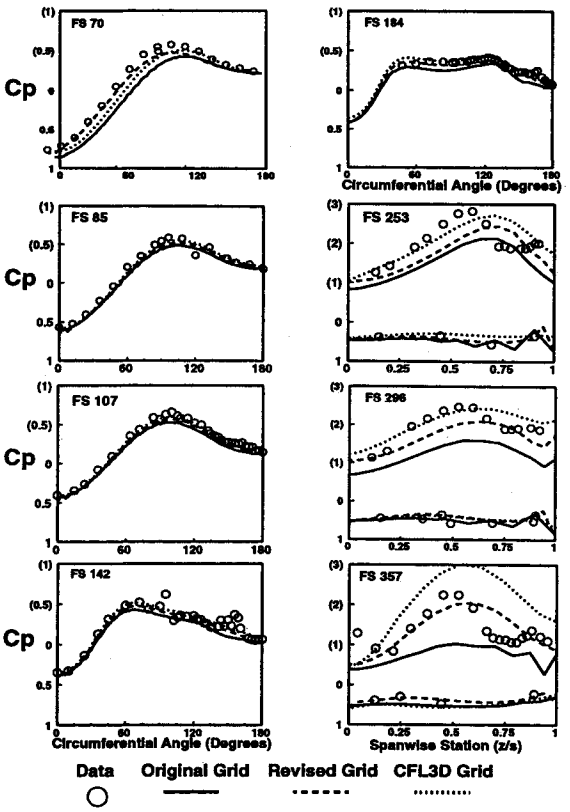

Fig. 5 Surface static pressure distributions.

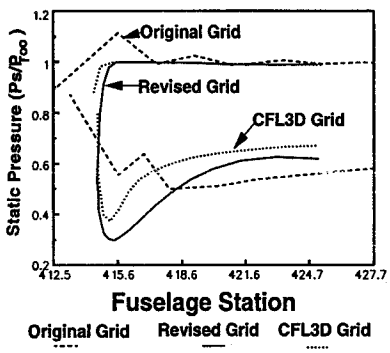

Fig. 6 Cowl highlight surface static pressure distributions at 180 deg (bottom of cowl).

The surface static pressure distributions about the inlet highlight obtained from the three solutions are shown in Fig. 6. The distribution obtained using the embedded c-grid is much improved over the original solution. It should be noted that the pressure distribution obtained with the original grid without the c-grid does not adequately resolve the supersonic acceleration about the highlight and there is a significant total pressure overshoot (10% greater than freestream).

The CFL3D pressure distributions compare much closer with those obtained by PARC3D using an embedded c-grid about the inlet highlight than the original grid results. The poor pressure distributions obtained with PARC3D without a c-grid about the leading-edge highlight may be due to the

presence of a discontinuity, in the grid distribution in the axial direction, at the inlet entrance grid block interface that extends into the upstream flowfield. Due to the complex geometry, manually extending the grid interface to maintain continuous metrics is difficult. Also, the number of grid points in the region of the highlight for the original grid is approximately one-half the number used in the CFL3D grid.

The predicted total pressure contours at the inlet entrance obtained for the two PARC3D solutions are shown in Fig. 7. The boundary layers are significantly thinner for the revised grid results as compared to the original grid solution. This improvement is due to the c-grid providing better resolution of the flow gradients about the lip highlight. These gradients are severe since the stagnation point is located along the outside of the inlet lip region and flow must be turned 180 deg as it enters the inlet. The total pressure contours obtained from the CFL3D results (not shown) indicate a slightly thicker boundary layer than that obtained with PARC3D using the embedded c-grid. However, the losses associated with the CFL3D solution appear to be somewhat lower than the PARC3D results obtained without the c-grid. A region of crossflow separation is shown in the revised grid and CFL3D grid solutions. The original grid does not indicate such a region. The improved resolution of the inlet highlight region appears to be the reason this feature is resolved in the revised grid and CFL3D grid results.

The revised grid solutions using PARC3D and CFL3D (not shown) indicate a region of cross-stream separated flow along the lip shown in Fig. 7. For the revised grid and CFL3D grid results this region is located along the outboard wall of the lip and migrates towards the bottom of the duct and merges with vortices that migrate from the inboard corners of the duct. For the original grid results, this separated region is not present. This difference is attributed to the increased grid resolution in the revised grid that utilizes an embedded c-grid around the inlet highlight. However, a similar result was obtained with CFL3D that did not have the embedded c-grid. The streamwise number of grid points was approximately doubled in the highlight region, which may also provide sufficient improvement in surface resolution. This issue was noted in regards to the static pressure distributions about the inlet highlight (Fig. 6). These vortices appear to be major contributors to the development of the inlet duct secondary flowfield. This indicates that the effect of the lip does have a significant impact on the development of the secondary flowfield in inlets. This migration was exhibited by using the animation capabilities of the FAST program.[17] It should be noted that these vortices contain very low energy flow and are significant contributors to the high levels of distortion that have been predicted at the engine face. Since data is not available to confirm that these vorticies exist, they may not be real or as intense and may be attributed to a lack of adequate inlet highlight resolution. This region of cross-stream separation is not present in calculations for this inlet with a freestream Mach number of 0.4 or higher. At these higher Mach numbers, the captured stream tube stagnation line is placed on the inside of the inlet highlight and the flow does not turn 180 deg to enter the inlet. More recent calculations using the Baldwin–Barth turbulence model indicate the presence of this cross-stream separation, although its strength is somewhat attenuated.

The predicted total pressure contours at the engine face, are shown in Fig. 8. The PARC3D results obtained with the revised grid are much less distorted than those obtained with the original grid. The major difference is the presence of the embedded c-grid about the inlet highlight in the revised grid, which has a significantly higher grid density in the highlight region. This c-grid provided much lower losses at the inflow to the inlet, and therefore, the losses and distortions are reduced at the outflow station. Also, the original grid solution indicates that the LEX vortex has migrated to the compressor face. With the revised grid, the LEX vortex is ingested, but migrates into the inboard wall of the inlet duct. This change in vortex movement is attributed to the improved modeling of the upper diverter.

A comparison of the predicted inlet performance using a 40-probe simulation for both grids with PARC3D to data[7] is shown in Table 2. As can be seen, the results obtained using the revised grid indicate improved inlet performance over the original grid and much closer agreement to the average data than the original grid results. The flow rates did not exactly match the measured rates due to difficulties in setting the exit static pressure to a value that results in the exact measured flow rate. Each time the static pressure is adjusted, the solution requires a few thousand iterations to adjust to the revised downstream boundary conditions.

The revised grid PARC3D-predicted distortions $[(P_{T\max} P_{T\min})/P_{T\text{avg}}]$ are less than the CFL3D predictions (not shown). Part of these distortions may be attributed to the lack of a c-grid around the inlet highlight for the CFL3D calculations. The use of the c-grid improved the PARC3D calculations significantly. In Table 2, a comparison of the CFL3D-predicted inlet performance to the PARC3D-revised grid results shows that the CFL3D predictions have a lower recovery $(P_{T\text{avg}}/P_{T\infty})$ and significantly higher distortion than the PARC3D results. Vortex shear layer distortion in the region of the pole of the CFL3D solution is the major contributor to the high level of distortion.

A comparison of the PARC3D normalized total pressure contours at the compressor face using the revised grid are compared to data obtained with a 19.2% scale model for the

Table 2 Inlet performance summary (rake simulation)

	Original grid	Revised grid	CFL3D	Data
Full-scale corrected flow rate	146.7	144.7	142.6	143.5
Model scale recovery	87.9%	91.9%	90.1%	94.5%
Model scale distortion	31%	24%	30%	12%
Engine face Mach number	0.46	0.45	0.45	0.45

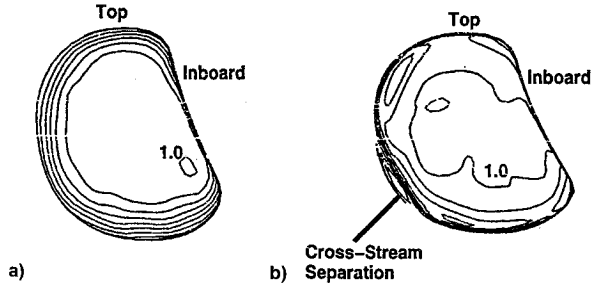

Fig. 7 Inlet entrance total pressure contours ($P_T/P_{T\infty}$) PARC3D results: a) original and b) revised grids.

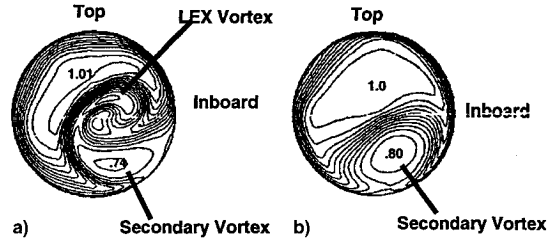

Fig. 8 Engine face total pressure contours ($P_T/P_{T\infty}$): PARC3D results: a) original and b) revised grids.

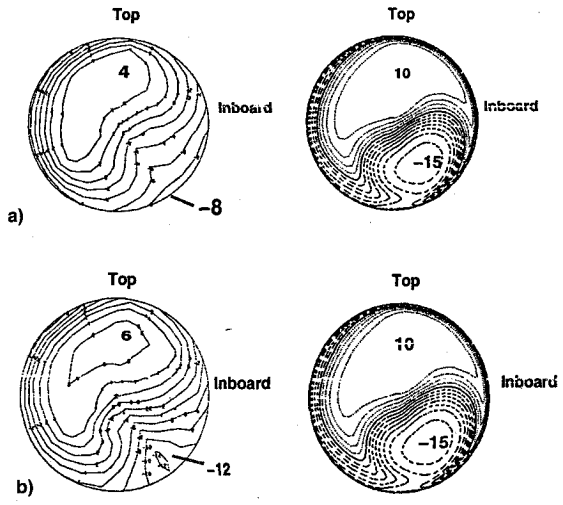

Fig. 9 Engine face normalized total pressure contours ($P_T - P_{T_{avg}}/P_{T_{avg}}$) looking upstream. Comparison to measured a) average and b) dynamic distortions.

F/A-18A aircraft with a freestream Mach number of 0.2 (Ref. 7) in Fig. 9. The PARC3D contours are presented using the full computational grid in order to obtain smooth contours. The use of the 40-probe rake simulation produced linear interpolations between data points when using PLOT3D. It is not known what type of interpolation scheme was used for the experimental rake data to obtain the smooth contours. The normalized total pressure represents the percent deviation from the rake-averaged total pressure at the engine face. In Fig. 9a, the measured time-averaged normalized total pressure is shown and the measured normalized total pressure at instantaneous peak distortion at maximum fan sensitivity is shown in Fig. 9b. As can be seen, there is a significant difference between the two experimental results. This indicates that a large amount of unsteadiness may be present in the inlet duct flowfield. The PARC3D results appear much more similar to the peak distortion data than the time-averaged experimental result. It should be noted that the solutions obtained are converged to an asymptotic, non-time-varying condition and not time accurate, therefore, the solutions obtained cannot duplicate the time-averaged data shown or the peak distortion data. In order to attempt to match the time-averaged data, a time accurate solution is needed with the results averaged.

Numerical Issues

A comparison of the numerical performance of the two codes, shown in Table 3, indicates that CFL3D is faster, but requires significantly more in-core memory than PARC3D. This is due to the fact that CFL3D stores all of the numerical data in core memory, whereas PARC3D keeps only the current grid block data in core memory and writes the rest to disk memory. Although difficult to assess, both codes required approximately the same amount of computational time to obtain a converged solution. Some differences in CPU time may be attributed to PARC3D requiring much more I/O than CFL3D, since data for only one grid block is stored in core memory using the PARC3D code. The drop in the residuals for both codes was similar. The residuals for the viscous blocks dropped approximately three orders of magnitude, whereas the inviscid blocks dropped up to six orders of magnitude. Since the solutions obtained are the result of many restarts and corrections, and consist of many grid blocks, convergences plots of residuals were not obtained.

The calculations of lift and drag using the revised grid for PARC3D and CFL3D as a function of iterations indicate the CFL3D solution has less steady-state convergence than the PARC3D solution. The lift and drag coefficients calculated for PARC3D were virtually constant. The CFL3D lift coefficient varied by $\pm 3.5\%$ and the drag coefficient varied by $\pm 1.5\%$. The major source of this oscillation in lift and drag is the leeward side of the wing. A difference in the PARC3D and CFL3D flowfield solution convergence was found in the inlet duct flowfield calculation. The CFL3D-predicted mass flow rate varied $\pm 1\%$, whereas the PARC3D-calculated mass flow rate variation was $\pm 0.4\%$ as the solution was iterated.

Table 3 Code performance summary (Cray Y-MP computer)

	CFL3D	PARC3D
Grid points	911,204	1,214,207
Speed (10^{-6} s/iter/point)	18.2	27.3
Core memory (MWords)[a]	28.9	6.5
Words/point	31.7	32.4

[a]For PARC3D, this is the memory required for the largest grid block.

Conclusions and Recommendations

The PARC3D forebody/fuselage surface static pressures compared well with the flight test data and showed an improvement over the original grid results. The inclusion of the diverter and slot in the revised grid solution had an effect on the path followed by the under LEX vortex. The forebody/LEX surface static pressures obtained with CFL3D compared well to the PARC3D results and with data.

Also, the refined definition of the upper diverter region above the inlet cowl appears to have had a significant influence on the migration of the ingested vortex. The original grid indicates that the vortex migrates to the compressor face, whereas the revised grid indicates that the vortex dissipates along the inboard wall of the inlet duct. The PARC3D inlet flowfield calculations, using the revised grid, show a significant improvement in the recovery and distortion over the original grid. This improvement appears to be due to the improved modeling of the inlet highlight and upper diverter region. However, PARC3D still overpredicts the inlet flow distortion and underpredicts the inlet total pressure recovery. Further refinements to the highlight grid may reduce the distortion. The use of other turbulence models that handle vortical flows better than the Baldwin–Lomax turbulence model may improve the mixing of the high- and low-energy flows. The unsteadiness of the inlet flowfield may require the use of a time-accurate solution.

The effects of the inlet lip appear to have a significant effect on the development of the inlet duct secondary flowfield. The vortices generated along the inlet highlight may be either fictitious or less intense and may be due to a lack of adequate grid resolution or turbulence modeling capability.

Acknowledgments

Support of this work by the NASA Lewis Research Center under Contract NAS3-25266 is gratefully acknowledged. The interest shown by Project Manager, Richard R. Burley, is particularly appreciated. The excellent grid generation work provided by James E. Bruns is also noted. In addition, the authors thank James R. Sirbaugh for his suggestions concerning multigridding with CFL3D and Raymond R. Cosner of McDonnell Aircraft Company for his help in obtaining the F/A-18A airframe geometry database.

References

[1]Ghaffari, F., Bates, B. L., Luckring, J. M., Thomas, J. L., and Biedron, R. T., "Navier-Stokes Solutions About the F/A-18 Wing-LEX-Fuselage Configuration with Multi-Block Structured Grids,"

AIAA Paper 91-3291, Sept. 1991.

[2]Gee, K., Tavella, D., and Schiff, L. B., "Computational Optimization of a Pneumatic Fuselage Forebody Flow Control Concept," AIAA Paper 91-3249, Sept. 1991.

[3]Burley, R. R., Anderson, B. H., Smith, C. F., and Harloff, G. J., "High Alpha Inlets," Aeropropulsion '91, LeRC, NASA CP 10063, Cleveland, OH, March 1991.

[4]Bruns, J. E., and Smith, C. F., "Full Navier-Stokes Calculations on the Installed F/A-18 Inlet at a High Angle of Attack," AIAA Paper 92-3175, July 1992.

[5]Cooper, G. K., and Sirbaugh, J., "The PARC Distinction: A Practical Flow Solver," AIAA Paper 90-2002, July 1990.

[6]Fisher, D. F., Banks, D. W., and Richwine, D. M., "F-18 High Alpha Research Vehicle Surface Pressures: Initial In-Flight Results and Correlation with Flow Visualization and Wind-Tunnel Data," NASA TM 101724, 1990.

[7]Amin, N. F., Hollweger, D. J., Franks, W. J., De la Vega, E. G., Yamada, M., and Tsukahira, T. W., "AEDC Series 1 F-18, .192 Scale Inlet Analysis Report," Northrop Corp., Aircraft Div., NOR 77-310, Hawthorne, CA, May 1977.

[8]Thomas, J. L., Taylor, S. L., and Anderson, W. K., "Navier-Stokes Computations of Vortical Flows over Low Aspect Ratio Wings," AIAA Paper 87-0207, Jan. 1987.

[9]Baldwin, B. S., and Lomax, H., "Thin Layer Approximation and Algebraic Turbulence Model for Separated Turbulent Flows," AIAA Paper 78-257, Jan. 1978.

[10]Sirbaugh, J. R., and Reichart, B. A., "Computation of a Circular-to-Rectangular Transition Duct Flow Field," AIAA Paper 91-1741, June 1991.

[11]Stokes, M. L., and Kneile, K. L., "A Search/Interpolation Algorithm for CFD Analysis," World Congress on Computational Mechanics, Univ. of Texas, Austin, TX, Sept. 1986.

[12]Bierdron, R. T., and Thomas, J. L., "A Generalized Patched-Grid Algorithm with Application to the F-18 Forebody with Actuated Control Strake," *Computing Systems in Engineering*, Vol. 1, Nos. 2–4, 1990, pp. 563–576.

[13]Anderson, W. K., "Implicit Multigrid Algorithms for the Three-Dimensional Flux Split Euler Equations," Ph.D. Dissertation, Mississippi State Univ., Mississippi State, MS, Aug. 1986.

[14]Steinbrenner, J. P., Chawner, J. R., and Fouts, C. L., "The Gridgen 3-D Multiple Block Grid Generation System," Wright Research and Development Center, WRDC-TR-90-3022, July 1990.

[15]Smith, C. F., and Podleski, S. D., "Installed F/A-18 Inlet Flow Calculations at 30 Degrees Angle-of-Attack: A Comparative Study," NASA CR 195297, April 1994.

[16]Walatka, P. P., Buning, P. G., Pierce, L., and Elson, P. A., "PLOT3D User's Guide," NASA TM 101067, March 1990.

[17]Walatka, P. P., Plessel, T., McCabe, R. K., Clucas, J., and Elson, P. A., "FAST User's Manual," NASA Ames Research Center: WAO and RND, Beta 2.0, RND-91-011, Dec. 1991.

[18]Amin, N. F., Richards, C. J., De la Vega, E. G., and Dhanidina, M. A., "F/A-18A Engine Inlet Survey Report, Vols. 1, 2, and 3," Northrop Corp., Aircraft Div., NOR 81-316, Hawthorne, CA, Nov. 1981.